研 究 論 文
大 韓 溶 接 學 會 誌
第 9 卷 第 2 號 1991年 6月
Junrnal of the Korean
Welding Society
Vol. 9, No. 2, Jun., 1991

AISI 316 스테인레스강의 CO_2 레이저 용접

김 재 도*

High Power CO_2 Laser Beam Welding of AISI 316 Stainless Steel

J.D. Kim*

Key Words : Laser Beam Welding(레이저 빔 용접), Stainless Steel(스테인레스 강), CO_2 Laser(CO_2 레이저), Heat Flow Equation(열전달 방정식), Hot Cracking(고온 균열), Porosity(기공)

초 록

6mm 두께의 AISI 316 스테인레스강의 레이저 용접 특성에 대해서 고찰하였다. 3kW CO_2 레이저를 사용하였으며, 레이저 빔은 TEM_{00} 모우드였고 연속파이었다. 용입 깊이, 비드 폭, 고온 크랙, 기공등의 특성을 고찰하는데 있어서, 레이저 출력은 1kW에서 2.5kW까지, 용접 속도는 5.1m/min까지 적용하였다. 3차원 열전달 방정식에 의한 용입 깊이와 비드 폭에 대한 예측치와 실험 결과를 비교하였는데, 서로 잘 일치하였다.

1. Introduction

High power laser beams are used in a wide variety of materials processing applications such as cutting, welding, drilling and surface treatment. The CO_2 laser is increasingly used in laser beam welding because of the highly potential advantages. High power laser welding is a high energy density, no filler metals and low heat input process to join metals. As the comparison with the conventional welding, precision work and good fit-up to join the metals are required and maintenance is expensive at present[1,2,3].

The principal variables of laser beam welding are the laser beam power, travel speed and beam spot size. The penetration depth during laser beam welding is directly related to the power density of the laser beam. Generally, for a constant beam size, the penetration depth increases with increasing laser beam power.

Though fast acceptance of high power laser applications by the manufacturing community has been increased, data are lacking in laser welding

* 정회원, 인하대학교 공과대학 기계공학과

of stainless steels. The results of laser beam welding are dependent upon the lasers, which include the wavelength of beam, beam mode and maximum laser power. The objective of this investigation is to evaluate the welding parameters for the AISI 316 stainless steel, the microstructures and the welding defect such as porosity.

The effects of laser beam welding depend upon many variables, some of which are not easy to control or monitor. Therefore, it is very useful to theoretically predict the experimental trends to establish the understanding of laser welding process. In penetration welding it is important to be able to predict the maximum possible penetration depth for given sources and to calculate the effects of varying any parameter.

2. Heat Flow Equation

Many solutions to the heat conduction equations with different source terms have been analytically or numerically given by many authors[4~8]. Three-dimensional solution for the heat flow in laser beam welding with a constant moving Gaussian heat source has been introduced to predict the penetration depth and bead width in stainless steel.

The laser beam is parallel to the z-axis and moves in the x-direction at a constant velocity, v, as shown in Fig. 1. In the material, the laser beam is attenuated with an absorption coefficient α. In general, the laser beam turned on at time $-t_1$ and turned off t_2. Heat loss from the surface of materialis assumed to be negligible compared to conduction into the material. The thermal conductivity(K), density(ρ), and specific heat(C) are assumed to be independent of temperature[9,10].

The time dependent heat diffusion equation is

$$\nabla^2 T = \frac{1}{\kappa}\frac{\partial T}{\partial t} - \frac{G}{K} \qquad (1)$$

where κ is the thermal diffusivity and G is the heat source function which is defined as follows[9,10].

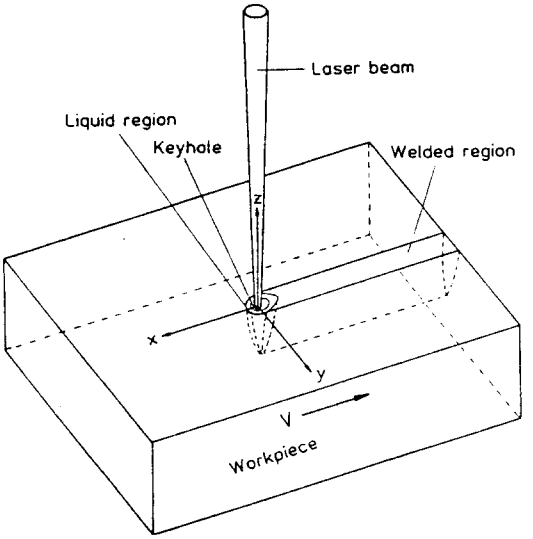

Fig. 1 Schematic illustration of laser beam welding by a Gaussian laser beam moving in the x-direction at a constant velocity

$$G = \frac{2\alpha(1-R)p}{\pi\delta^2}\exp\{-2(x-vt)^2/\delta^2 - 2y^2/\delta^2 - \alpha z\} \qquad (2)$$

in which p is the incident laser power, R is the reflectivity, and δ is the radius of beam spot. The solution is expressed in terms of normalized variables where $\chi = \sqrt{2}x/\delta$, $\xi = \sqrt{2}y/\delta$, $\zeta = \alpha z$, $\tau = 8\kappa t/\delta^2$, $\nu = v\delta/4\sqrt{2}\kappa$, and $\gamma = \alpha\delta/2\sqrt{2}$.

$$T(x, y, z, t) = [p(1-R)/2\sqrt{2}\pi K\delta] \cdot \theta(\chi, \xi, \zeta, \tau, \nu, \gamma) \qquad (3)$$

$$\theta(\chi, \xi, \zeta, \tau, \nu, \gamma) = (\gamma/2\sqrt{\pi}) \int_{\tau_0}^{\tau+\tau_1} [\exp(\gamma^2\tau')/(\tau'+1)]\exp[-\{(\chi-\nu(\tau-\tau'))^2+\xi^2\}/(\tau'+1)] [\exp(\zeta)\mathrm{erfc}(\gamma\sqrt{\tau'}+\zeta/2\gamma\sqrt{\tau'}) + \exp(\zeta)\mathrm{erfc}(\gamma\sqrt{\tau'}+\zeta/2\gamma\sqrt{\tau'})]d\tau'$$

where $\tau_0 = 0, \quad -\tau_1 < \tau < \tau_2$

$= \tau - \tau_2, \quad \tau > \tau_2$

and θ is the normalized temperature rise.

The average values[11] of the thermophysical properties of AISI 316 have been used for calculation as shown in Table 1.

Table 1 The average values of physical properties of AISI 316

Thermal conductivity (W/cm℃)	0.24
Thermal diffusivity (cm/sec)	0.045
Absorption coefficient (cm^{-1})	6.0
Reflectivity	0.3
Vaporizing point (℃)	2870
Melting point (℃)	1500

3. Experiments

3.1. Materials and laser system

The specimens of 6mm thick AISI 316 steel consisted of rectangular sheets, 200mm long and 100mm wide. The surface condition of material for bead-on plate weld was mill finish. The chemical compositions of the materials are shownin Table 2.

Table 2 Chemical compositions of stainless steel

(wt %)

	C	Mn	Si	P	S	Cr	Ni	Mo	Nb
AISI 316	0.054	1.65	0.49	0.02	0.012	17.1	12.5	2.23	0.005

This work has been carried out using a continuous wave 3kW CO_2 laser which is of a fast axial flow type and is linked to a working station including a NC table. The laser beam is reflected down and focused by a ZnSe lens with a focal length of 127mm. A copper nozzle can be adjusted and replaced easily. Fig.2 depicts the typical coaxial optic/nozzle system. The incident beam power is reduced by about 20% of output beam power because of the beam divergence and the absorption of the optic system during delivering from the laser system to the working station[12].

3.2. Laser beam welding

The laser power ranged from 1.0 to 2.5kW and the travel speeds were 0.5, 1.0, 1.5, 2.1, 3.0, 4.2 and 5.1m/min at each power level. The laser mode was

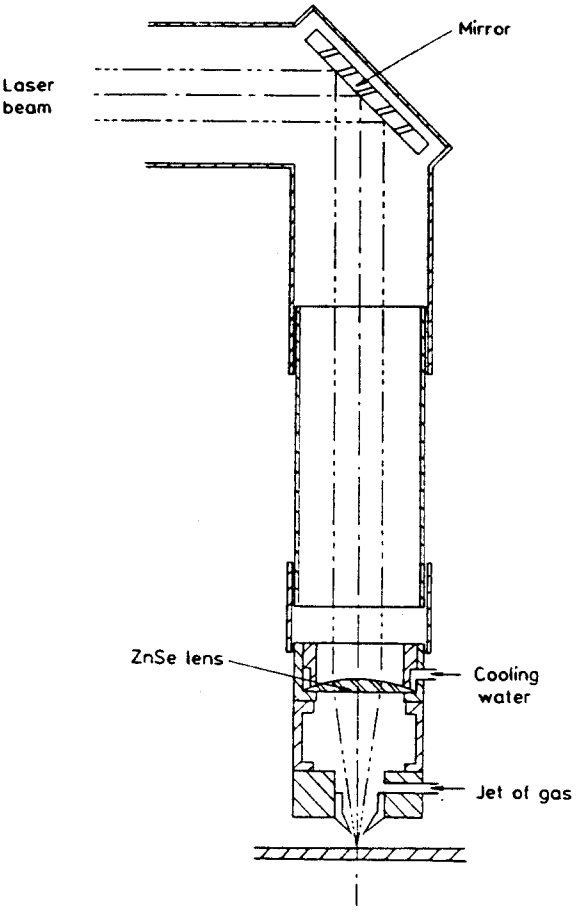

Fig. 2 Typical coaxial optic/nozzle system with gas shielding assist

almost TEM_{00} beam (Gaussian beam). The intensity distribution of unfocused beams were investigated by vaporizing transparent acrylic material as shown in Fig. 3. The acrylic burn print gave an information on the distribution of beam energy. The specimens were degreased with acetone just before laser melting. The focal position was 1.0mm below the surface of material because the optimum focal position is between 0.5 and 1.5mm below the surface of material in this laser system[12]. Argon was used as a shielding gas with a flow rate of 10 l/min.

To measure the penetration depth and the bead width, transverse sections were taken 50mm from

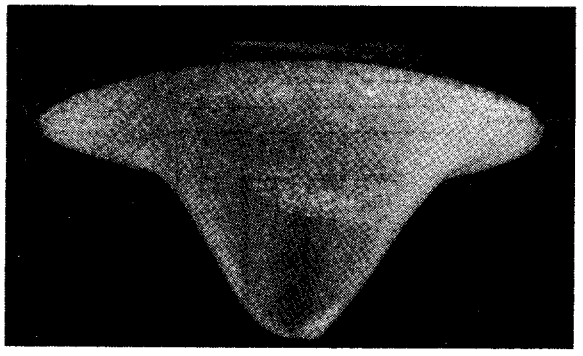

Fig. 3 Stationary deep unfocused beam print in acrylic

the end of each melt. The mounted specimens were polished and etched chemically using Glyceregia solution. An optical microscope was used to measure the penetration depth and the bead width. A Forster ferrite measurement equipment was used to measure the content of delta ferrite in the laser welds. An energy dispersive analysis with X-ray (EDAX) and a scanning electron microscopy (SEM) were used to reveal the cause of the cracks which occurred during laser beam welding of stainless steels.

4. Results and Discussion

4.1. Penetration depth and bead width

The experimentally obtained penetration depth and bead width in AISI 316 steel as shown in Fig. 4. It can be seen that the penetration depth decreases exponentially with the travel speed. Similarly, at a fixed travel speed the penetration depth is proportional to the laser power. As the travel speed increases and the laser power decreases, the penetration depth and bead width decrease due to the lower heat input. As the travel speed decreases at a constant laser power, the extent of the molten metal zone surrounding the keyhole increases in proportional to the increased heat input. Eventually, the metal vapor pressure is insufficient to counter the fluid dynamic forces of the liquid metal and the deep keyhole collapses. Under

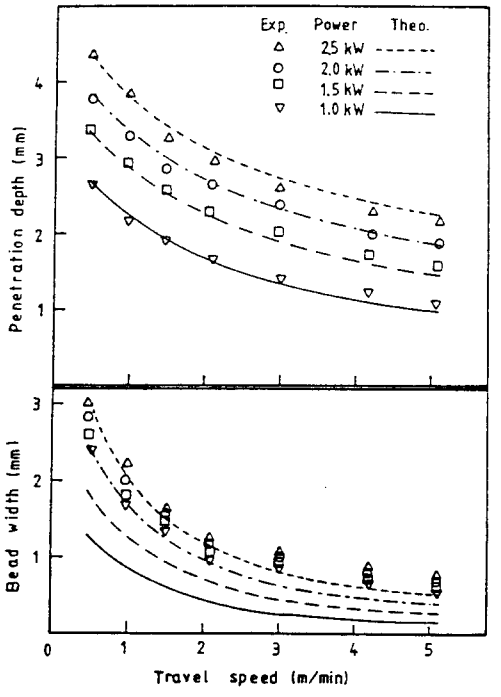

Fig. 4 Comparison of the experimental results with the theoretical model on penetration depth and bead width

sucha condition an abrupt decrease in penetration occurs at low travel speeds (less than 0.5m/min).

The calculated and experimentally obtained penetration depths are in good agreement with each other for this range of laser power and travel speed. But the experimentally obtained bead widths are wider than the calculated ones because of effect of plasma. At high travel speeds the calculated bead widths have a tendency to be narrower than the experimental ones whereas at low travel speeds the calculated ones are somewhat wider than the experimental ones. The plasma produced during the laser beam welding acts like a secondary heat source above the keyhole, causing a wide weld bead. In fact, it was experienced that the plasma produced during laser beam welding was more serious in stainless steel than in carbon steel.

The ratio of penetration depth to bead width is illustrated in Fig.5. The ratio increases with increasing travel speed in the studied range. The

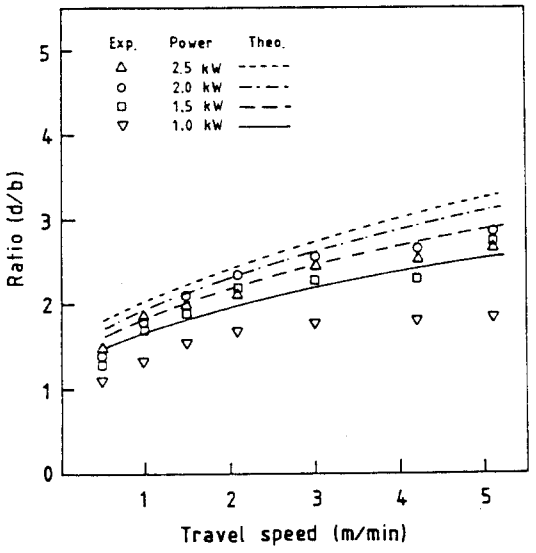

Fig. 5 The ratio as a function of travel speed at various laser powers

Fig. 6 Macrosection of laser weld in AISI 316 steel (Laser power, 2kW, travel speed, 3.0m/min, x25)

predicted ratios are higher than the experimental ones. As the laser power increases, the calculated ratio increases. At high travel speed the high ratio is achieved. The typical macroseciton of laser welds in stainless steel is shown in Fig. 6. The bead shape adopted at low travel speeds is like a nail head. Fig.7 shows a good agreement between the

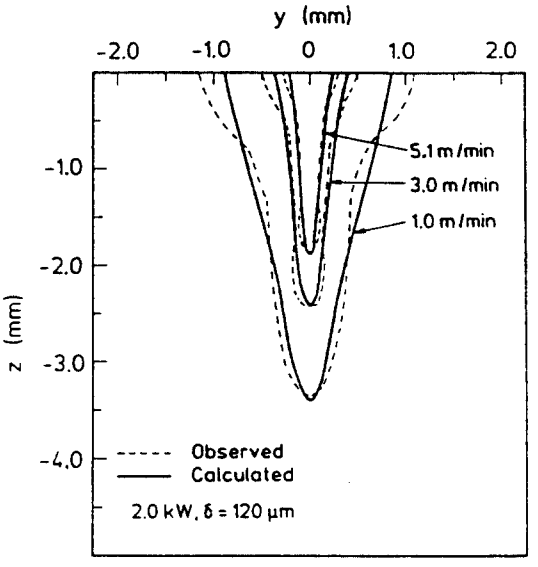

Fig. 7 Comparison between the calculated and observed fusion boundaries of laser welds with various travel speeds

calculated and observed fusion boundaries based on the beam spot radius of 120μm. As the travel speed increases, the calculated fusion boundary is slightly narrower than the observed one whereas it is somewhat wider with decreasing travel speed.

4.2. Microstructures

The laser weld microstructure of AISI 316 is almost entirely fine austenite throughout the laser welds as expected by a prediction method of Suutala[13] in Fig. 8. The planar-to-cellular transition is fairly typical of laser welds for austenitic stainless steel. Grain size in heat-affected zone for stainless steel remains unchanged from the parent material. The microstructure of laser welds in AISI 316 steel was predominantly cellular dendrite, with the size of the cells decreasing with increasing travel speed. The fusion boundary was clearly defined with cellular dendritic solidification extending directly from the fusion boundary.

4.3. Hot cracking

A singnificant problem of stainless steel welding

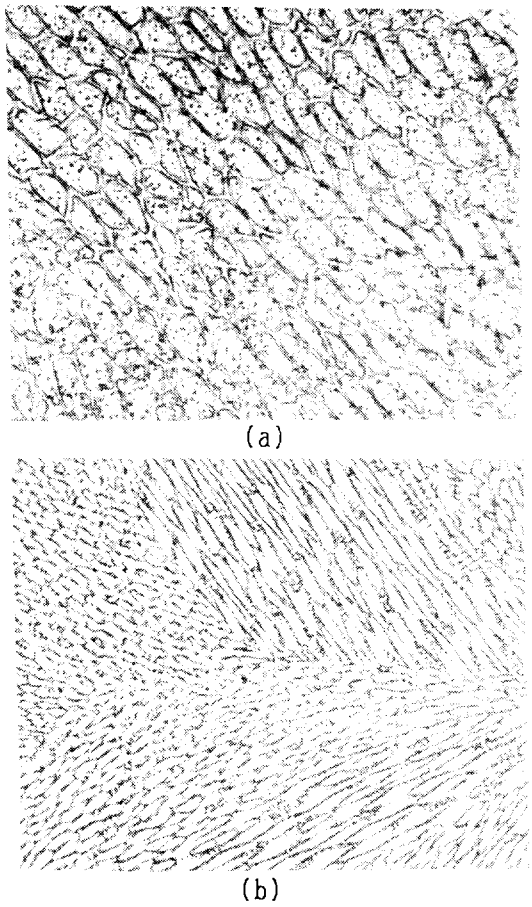

Fig. 8 Microstructures of laser welds in AISI 316 steel
(a) Laser power, 2kW, travel speed, 0.5m/min, x500.
(b) Laser power, 2kW, travel speed, 3.0m/min, x500.

is a tendency toward hot cracking. To minimize this tendency, small amounts of delta ferrite are produced in the as-welded microstructure.

Hot cracking in laser welds of AISI 316 steel was found at high travel speeds, 3.0, 4.2, and 5.1m/min at laser powers of 2.0 and 2.5kW, and generally occuring in the bulk weld metal or close to the fusion boundary illustrated in Fig. 9. It was found that sulphur was enriched in the crack by using SEM and EDAX. This suggests that the segregation of sulphur to dendrite boundaries is probably the main cause of the development of hot cracking in laser welds of AISI 316 steel even though some

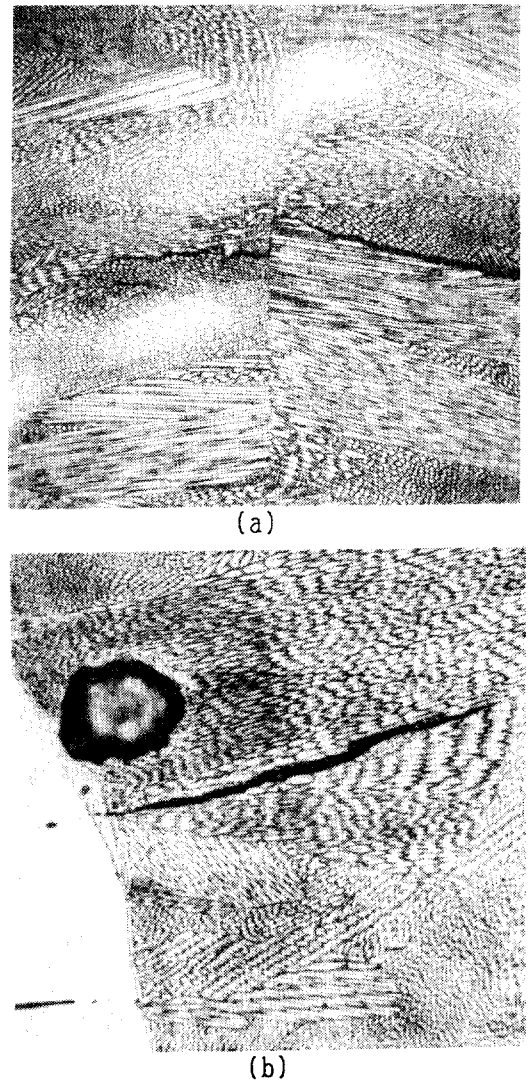

Fig. 9 Hot crackings of laser welds in AISI 316 steel.
(a) Laser power, 2kW, travel speed, 4.2m/min, x240,
(b) Laser power, 2kW, travel speed, 5.1m/min, x500.

authors[14,15] reported that the risk of hot cracking is limited when laser welding speed is high. Weld metal hot cracking was observed interdendritic, i.e., they follow the boundaries of the solidification structure.

The high travel speed during the laser beam welding affects the risk of hot cracking due to the very fast cooling. Although high solidification rate

can decrease hot cracking sensitivity by reducing segregation of harmful elements, high solidification rate can also increase hot cracking sensitivity by impending the formation of delta ferrite in stainless steel welds because solidification to ferrite is beneficial for increasing hot cracking resistance. It is well-known that fully austenitic weld metal is generally most sensitive to hot cracking.

4.4. Porosity

Weld porosity is a major problem in high energy density welding, depending on the materials. Once the laser beam makes a keyhole in the material, the weld joint penetration can be so deep that the metal vapor, decomposition of inclusions or shielding gas can be trapped in the quickly solidifying molten weld pool before it can float to the top of the weld pool and escape. This results in laser weld porosity.

The porosity consisted of fine bubbles and were distributed at the lower portion of welds or at near the fusion boundary as shown in Fig.10. The porosities in partial penetration welds were seen at the lower portion of fusion zone with no relation of laser power and travel speed.

It is believed that fine porosity at lower portion or near the fusion bounary is a result of decomposition of inclusions to from carbon monoxide or a result of entrainment of atmospheric oxygen. In laser beam welding the keyhole is filled with metal vapor at very high temperature. As the volume of weld metal is small and very vigorous stirring of the weld pool occurs, all of the molten metal will be raised to a very high temperature at some time during the formation of the weld. All oxides will tend to be reduced by C to form CO above 2000℃[16,17]. This reaction will contribute to the fusion zone purification effect and is presumably the cause of the reduction in weld metal C, and O contents. The gas, CO, forming the pores may be also formed as a result of atmospheric oxygen being entrained into the weld. In fact, the high energy density welding process such as electron beam welding or laser beam welding, in which the weld pool is molten for only a very short time, does not allow much time for degassing.

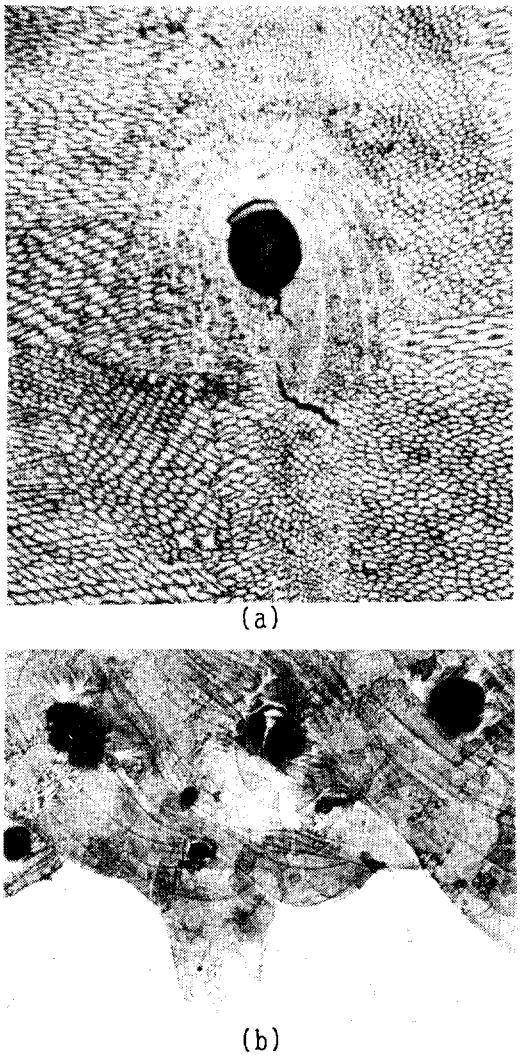

Fig. 10 Porosities of laser welds in AISI 316
(a) Pore in the center of laser weld, x500,
(b) Pores of partial penetration weld in longitudinal section, x200.

5. Conclusions

The 6mm thick AISI 316 steel was melted as bead-on-plate weld in order to find the characteristics of penetration and microstructures, using a continuous wave 3kW CO_2 laser with the various travel speeds. The ratio of penetration depth to

bead width in laser welds of AISI 316 has a tendency of steady increase with increasing travel speed in the studied range. The microstructure was almost entirely fine austenite throughout the laser welds of AISI 316, and was predominantly cellular dendrite with the size of the cells decreasing with increasing travel speed. Hot cracking in laser welds of AISI 316 steel was found even at high travel speeds, occurring in the bulk weld metal or close to the fusion boundary. It also found that the cracking occurred interdendritic and was probably caused by sulphur segregation during the solidification.

Acknowledgments

This paper was supported by NON DIRECTED RESEARCH FUND, Korea Research Foundation, 1990. The author wishes to thank the financial support.

References

1) R. Walker: Applying multikilowatt CO_2 lasers in industry, Lasers & Applications, Vol. 4, (1984), pp. 61-69.
2) D.M. Hull and A. Stewart: Laser beam profiles, principles and definitions, Lasers & Applications, Vol. 10, (1985), pp. 75-80.
3) R.J. Bruno et al.: Laser beam shaping for maximum uniformity and minimum loss, Lasers & Applications, Vol. 4, (1987), pp. 91-94.
4) D.T. Swift-Hook and A.E. Gick.: Penetration welding with lasers, Welding J., Vol. 52, No. 11, (1973), pp. 492s-499s.
5) P.G. Klemens: Heat balance and flow conductions for electron beam and laser welding, J. of Appl. Phy., Vol. 47, No. 5, (1976), pp. 2165-2173.
6) H.E. Cline and T.R. Anthony: Heat treating and melting material with a scanning laser or electron beam, J. of Appl. Phy., Vol. 48, No. 9, (1977), pp. 3896-3900.
7) J. Mazumder and W.M. Steen: Heat transfer model for CW laser material processing, J. of Appl. Phy., Vol. 51, No. 2, (1980), pp. 941-947.
8) M. Davies et al.: Modelling the fluid flow in laser beam welding, Welding J., Vol. 64, No. 7, (1985), pp. 167s-174s.
9) J.D. Kim and R.V. Subramanian: Heat flow in laser beam welding, Proc. of 4th Int'l Conf. of CIFFEL, Cannes France, (1988), pp. 175-182.
10) J.D. Kim: Prediction of the penetration depth in laser beam welding, KSME journal, Vol. 4, No. 1, (1990), pp. 32-39.
11) Y.S. Touloukian: Thermophysical properties of high temperature solid materials, Vol. 1-6, The Macmillian Co., (1975).
12) J.D. Kim: High power CO_2 laser beam welding for low carbon steels, J. of KWS, Vol. 7, No. 4, (1989), pp. 12-21.
13) N. Suutala: Effect of solidification condition on the solidification mode in austenitic stainless steels, Met. Trans. 14A, No. 2, (1983), pp. 191-197.
14) G.M. Goodwin: The effects of heat input and weld process on hot cracking in stainless steel, Welding J., Vol. 67, No. 4, (1988), pp. 88s-94s.
15) S.A. David et al.: Effect of rapid solidification on stainless steel weld metal microstructures and its implications on the Schaeffer diagram, Welding J., Vol. 66, No. 10, (1987), pp. 289s-300s.
16) D.E. Nelson et al.: An investigation of weld hot cracking in duplex stainless steels, Welding J., Vol. 66, No. 8, (1987), pp. 127s-136s.
17) M.J. Cieslak: Hot cracking mechanism in CO_2 laser beam welds of dissimilar metals involving PH martensitic stainless steel sheet, Welding J., Vol. 66, No. 2, (1987), pp. 57s-59s.